Elsevier Editorial System(tm) for Engineering Geology
Manuscript Draft

Manuscript Number:

Title: Liquefaction potential in the May 20, 2012 Emilia, Italy, epicentral area: assessment and comparison with existing classifications

Article Type: Research Paper

Keywords: liquefaction, severity index, LPI, statistical analysis, Emilia, sand boils

Corresponding Author: Dr. George Papathanassiou, Ph.D.

Corresponding Author's Institution: Aristotle University of Thessaloniki

First Author: George Papathanassiou, Ph.D.

Order of Authors: George Papathanassiou, Ph.D.; Ambra Mantovani; Gabrielle Tarabusi; Dimitra Rapti; Riccardo Caputo

Abstract: Abstract
On 20th and 29th May 2012, two earthquakes occurred in Emilia-Romagna region (Northern Italy) triggering extensive liquefaction of the subsoil units. The consequences of liquefaction have been observed and reported by several agencies in a widespread area. The most impressive liquefaction manifestations were documented in a zone 3-4 km-long and 1 km-wide, where the villages of Sant'Agostino, San Carlo and Mirabello are located. The accurate existing post earthquake reports and the availability of geotechnical data provided by in-situ tests consist the basic ingredients for a reliable computation of the liquefaction potential parameters within this zone. In particular, the Liquefaction Potential Index (LPI) and Liquefaction Severtity Number (LSN) indexes were evaluated and then correlated to the occurrence or not of liquefaction phenomena. Thus, it was feasible to validate for one more time the existing classifications of the LPI and for the first time to apply and validate the proposed classification of LSN with the observed liquefaction-induced defromations. The outcome of this study shows that a threshold value of LPI equal to 13 or 14 is better to be taken into account instead of 5 for discriminating sites where liquefaction surface evidences should be expected from the non-liquefied ones. Moreover, from the correlation of the LSN valus with the occurrence of liquefaction it is concluded that the proposed threshold value of 10 fits statistically well with our dataset.

Suggested Reviewers: Resat Ulusay
resat@hacettepe.edu.tr

Harun Sonmez
haruns@hacettepe.edu.tr

Tomas Fernandez-Steeger
fernandez-steeger@lih.rwth-aachen.de

Thomas Holzer
tholzer@usgs.gov

Alessandro Michetti
alessandro.michetti@uninsubria.it

Highlights

Evaluation of liquefaction potential in the epicentral area of 2012 Emilia earthquake

Correlation of liquefaction-induced ground deformations with the values of LPI and LSN

Comparison of the outcome of this research with the existing classifications

Liquefaction potential in the May 20, 2012 Emilia, Italy, epicentral area: assessment and comparison with existing classifications

Papathanassiou G.[1,*], Mantovani A.[2], Tarabusi G.[2,3] , Rapti D.[2] and Caputo R.[2,4]

1) Dept. of Geology, Aristotle University of Thessaloniki, Greece

2) Dept. of Physics and Earth Sciences, Ferrara University, Italy

3) Istituto Nazionale di Geofisica e Vulcanologia, Rome, Italy

4) Research and Teaching Centre for Earthquake Geology, Tyrnavos, Greece

*) corresponding author: gpapatha@auth.gr

Abstract

On 20th and 29th May 2012, two earthquakes occurred in Emilia-Romagna region (Northern Italy) triggering extensive liquefaction of the subsoil units. The consequences of liquefaction have been observed and reported by several agencies in a widespread area. The most impressive liquefaction manifestations were documented in a zone 3-4 km-long and 1 km-wide, where the villages of Sant'Agostino, San Carlo and Mirabello are located. The accurate existing post earthquake reports and the availability of geotechnical data provided by *in-situ* tests consist the basic ingredients for a reliable computation of the liquefaction potential parameters within this zone. In particular, the *Liquefaction Potential Index* (*LPI*) and *Liquefaction Severtity Number* (*LSN*) indexes were evaluated and then correlated to the occurrence or not of liquefaction phenomena. Thus, it was feasible to validate for one more time the existing classifications of the *LPI* and for the first time to apply and validate the proposed classification of *LSN* with the observed liquefaction-induced defromations. The outcome of this study shows that a threshold value of *LPI* equal to 13 or 14 is better to be taken into account instead of 5 for discriminating sites where liquefaction surface evidences should be expected from the non-liquefied ones. Moreover, from the correlation of the *LSN* valus with the occurrence of liquefaction it is concluded that the proposed threshold value of 10 fits statistically well with our dataset.

Keywords: liquefaction, severity index, LPI, statistical analysis, Emilia

Introduction

The delineation of areas prone to liquefaction, the evaluation of their liquefaction potential and their detailed mapping represent crucial issues for mitigating the liquefaction risk and especially for minimizing or even avoiding the occurrence of structural damages at buildings. In the last decade, seismic microzonation studies including quantitative assessment of liquefaction hazard became a major task for urban areas or for areas planned for new buildings and/or infrastructures. Indeed, this has revealed an outstanding problem, for example, after the New Zealand, Canterbury 2010-1011 earthquake sequence, which started with the Darfield event in September 2010 (M_w = 7.1), followed during 2011 by other three major shocks close to Christchurch ranging from 5.9 to 6.3 (Tonkin and Taylor, 2010a; 2010b; 2013; Cubrinovski *et al.*, 2011; Orense *et al.*, 2011; Wotherspoon *et al.*, 2012; O'Rourke *et al.*, 2014).

In order to evaluate the liquefaction potential at a site and to compile liquefaction hazard maps, several approaches have been proposed in the past. The most widely applied is based on the *Liquefaction Potential Index* (*LPI* in the following), developed by Iwasaki *et al.* (1978). In addition, following the Christchurch seismic events and especially due to the widespread liquefaction that has occurred, a huge amount of in-situ tests have been performed in the broader epicentral area therefore allowing to propose a new approach referred to as the *Liquefaction Severity Number* (*LSN* in the following; Tonkin and Taylor, 2013; van Ballegooy *et al.*, 2014).

Recently, also the eastern sector of the Po plain, northern Italy, suffered diffuse and important liquefaction phenomena as a consequence of the May 20, and secondarily the May 29, 2012 earthquakes (Figure 1b; *e.g.* Caputo and Papathanassiou, 2012; Papathanassiou *et al.*, 2012; Di Manna *et al.*, 2012; Emergeo WG, 2013). Both magnitude (respectively M_w = 6.1 and 6.0; *e.g.* Pondrelli *et al.*, 2012) and focal depth (respectively, 6.3 and 10.2 km; http://iside.rm.ingv.it/) were comparable at least with the 2011 Christchurch events. Also in this case, several aftershocks up to M_w = 5.5 followed. Due to the similar dynamics of the two seismic sequences, as well as the general geological-stratigraphic setting of both epicentral areas characterized by alluvial plains with a flat morphology and a subsoil consisting of recent and poorly consolidated fluvial deposits, in this note we apply the two above mentioned parameters (*LPI* and *LSN*) to the Italian case study and correlate the obtained numerical results with the observed liquefaction phenomena. We additionally compare the estimated values with the existing classifications. At this regard it is worth of note that for the first time after it has been proposed, the *LSN* classification will be tested in an earthquake-induced liquefaction case based on a new dataset.

Seismotectonis of the epicentral area

The causative faults of the two mainshocks of the May 2012 Emilia sequence are two segments belonging to the Ferrara Arc, which represents the frontal most portion of the buried Northern Apennines fold-and-thrust belt (CNR, 1992; Figure 1a). As a first order feature of the continental accretionary wedge, it has a total length of more than 100 km. However, its internal geometry is particularly complex and highly segmented, where individual segments are commonly 10-30 km-long and characterized by different degrees of overstepping and overlapping geometries (Pieri and Groppi, 1981; Bigi *et al.*, 1982; Boccaletti *et al.*, 2004; Bonini *et al.*, 2014). The latter aspect is critical in determining the occurrence of soft or hard segment boundaries.

All these faults are seismogenic or at least capable of producing moderate-to-strong earthquakes depending on the possibility of a co-seismic linkage with the nearby segment(s). In any case, faulting along the Ferrara Arc is typically blind. As a consequence, during co-seismic reactivation the topographic surface is broadly deformed by a typical bulge associated with the fault-propagation folding process occurring at depth. Depending on the size of the fault, its dip-angle and the minimum depth of the sliding surface tip, the uplifted area has commonly an elliptical shape 10-30 km-long by 5-15 km-wide and a maximum vertical displacement of some tens of centimeters. The DInSAR technique applied to the Emilia sequence has clearly documented this phenomenon (*e.g.* Bignami *et al.*, 2012; Salvi *et al.*, 2012).

The repeating of similar 'areal morphogenic earthquakes' (*sensu* Caputo, 2005) during Late Quaternary locally caused cumulative effects in the otherwise flat morphology of the region. Depending on the energetic balance of single streams draining the alluvial plain, even small altimetric and gradient changes could generate river avulsions and diversions with the consequent abandonment of entire, several kilometers long, fluvial reaches and the shifting of the flooding events to different areas. These (palaeo)geographic changes are well reflected in the morphology of the region (MURST, 1997) where a careful inspection of the hydrographic network allowed to highlight the presence of several such drainage anomalies (*e.g.* Burrato *et al.*, 2003; 2012).

Due to the overwhelming regional scale subsidence affecting the Po Plain and the resulting high-rate sedimentary aggradation (Bartolini *et al.*, 1996), the above mentioned local uplifts and the following lateral mobility of the hydrographic network force the sedimentary architecture thus producing important stratigraphic variations. These quite evident in the deeper geology (Pieri and Groppi, 1981; Boccaletti *et al.*, 2004; Ghielmi *et al.*, 2010), but they could be also recognized within the shallow deposits (*e.g.* Calabrese *et al.*, 2012).

As a matter of fact, due to the persistence during the Holocene and even in historical times of this highly dynamic evolution (Bondesan, 1989), the present-day topography shows local altimetric differences up to several meters, while the shallow lithostratigraphic succession, say the first 10-20 m, is characterized by a complex 3D distribution of deposits and, of particular interest for the present

research, of the sandy and/or silty bodies. This complexity is also evident from a hydrogeological point of view, because the occurrence of isolated or, in contrast, connected sandy bodies may generate different acquifer systems characterized by semi-confined or confined conditions, commonly referred to as *A0* and *A1*, respectively, in the regional hydrogeological literature (*e.g.* Rapti-Caputo and Martinelli, 2009; Molinari *et al.*, 2007). As a consequence, the water content and the pore-pressure may also vary in space and time due to variable porosity and the related permeability distribution.

We will see in the following chapter that these sedimentary variations are crucial for explaining the occurrence or not of liquefaction phenomena at short distances even at sites with similar morphology and affected by the same ground acceleration.

The May 20 event

Seismic aspects

The strong ground motion generated by the May 20 earthquake induced severe structural damages to historical buildings, industries, farmhouses and ceramics warehouses. According to Galli *et al.* (2012) the macroseismic intensity scale was characterized by a maximum of VII (MCS) between Mirandola and San Felice sul Panaro and two distinct submaxima of VI-VII at Finale Emilia and San Carlo. The same authors locate accordingly the macroseismic epicentre closer to Finale Emilia. In general, residential houses suffered low-grade damage and very rare partial collapses and destructions due to their low vulnerability.

Based on the ESI-07 scale (Michetti *et al.*, 2007) a maximum environmental effects intensity of VIII was recognized in the area of San Carlo (Caputo and Papathanassiou, 2012; Di Manna *et al.*, 2012). The concentration of environmental effects, mainly associated with liquefaction phenomena, likely explains the cluster of damages and the attributed macroseismic intensity of VI-VII MCS at San Carlo.

Regarding the generated strong ground motion, a PGA value of 0.26 g for the horizontal component and 0.31 g for the vertical one was recorded at the station of Mirandola (MRN; Figure 1b), which is located at ca. 15 km distance from the May 20 instrumental epicenter (Bozzoni *et al.*, 2012; http://itaca.mi.ingv.it).

Liquefaction-induced deformation

As previously described, the investigated area is characterized by the presence of paleoriverbeds, out-flow channels and fans of the main Apennines streams crossing the area during he Holocene, which mostly controlled the distribution of the observed liquefaction phenomena. Similar scenarios have been generated in comparable alluvial settings for example in concomitance of the 1990 Luzon Philippines, the 2007 Niigaten Chuetsu-oki Japan and the 2010 Darfield New Zealand (Wotherspoon *et al.*, 2012) earthquakes, showing that this type of geological and geomorphological setting is

favourable to earthquake-induced surface ruptures and liquefaction phenomena.

For the aims of this paper, dedicated to compute the liquefaction potential indexes (*LPI* and *LSN*) and correlate them with the concomitant occurrence, or not, of liquefaction phenomena at the surface, we focus on two selected urban areas: Sant'Agostino and San Carlo, in the eastern epicentral sector, and Mirandola, on the western side; Figure 1b). Although the two areas have similar epicentral distances, the former experienced widespread liquefaction phenomena, like sand boils and ground fissures with ejection of silty sand-water mixtures and lateral spreading, while the western epicentral area generally did not, with only few exceptions.

In the eastern case study, the May 20 mainshock triggered locally important damages to lifelines (*e.g.* broken pipelines; Figure 2a), paved roads (*e.g.* decametric long cracks with opening up to several cm; Figure 2b) or buildings (*e.g.* cracking due to differential settlement; Figure 2c) (*e.g.* Papathanassiou *et al.*, 2012; Emergeo WG, 2013). Furthermore, earthquake-induced lateral spreading phenomena were reported in San Carlo and along the whole Sant'Agostino to Mirabello urban alignment (Figure 1b), inducing irrecoverable damages (Figure 2d) to houses built at the top of an abandoned natural levee (see previous section). At this regard, the topography of the natural levees though only few meters-higher than the surrounding alluvial plain played a crucial role, synergic with the co-seismic shaking and the liquefaction, in generating the clustering of the observed damage (Di Manna *et al.*, 2012).

A peculiarity of the region is also the presence of numerous large-diamater (ca. 1.5 m) water wells 5-10 m-deep generally connected with the first semi-confined acquifer (A0). Accordingly, during the main shock the ejection of large amounts of liquefied silty-sandy material was locally enhanced within courtyards of the residential buildings (Figure 3). This phenomenon generally caused the complete loss of functionality of the wells that sometimes remained completely filled by sand (Papathanassiou *et al.*, 2012), but also induced small size settlement of the nearby residential buildings as a consequence of ground loss (Figure 4).

Along the Sant'Agostino, San Carlo and Mirabello urban alignment, important ground ruptures tens of meters-long, with opening up to 20-30 cm and vertical offsets between the two blocks of 15-20 cm were also observed in the free field (*i.e.* affecting ploughed or natural soil; Figure 5). Fractures were commonly aligned parallel to the levee and locally formed overstepping and overlapping sets with a cumulative length of several hundred meters. In most cases, sandy material was ejected through these cracks (Figure 5b). Across one of such fracture systems a 50 m-long and 8 m-deep palaeoseismological trench has been excavated allowing to directly observe and log in detail the stratigraphy of the palaeo levee as well as the several subvertical dikes and other liquefaction associated features, like palaeo-slumps, graben structures and mixed-up sandy-silty layers (Caputo *et al.*, 2012a; 2012b). The results of trenching document the occurrence of palaeoliquefaction phenomena likely associated with the 1570 Ferrara earthquake.

During the post-seismic field survey, we also sampled ejected material for estimating their

granulometric distribution and Atterberg limits (analyses carried out at the Laboratory of Engineering Geology and Hydrogeology of the Department of Geology, Aristotle University of Thessaloniki). The majority of the ejecta are classified as SM with non-plastic fine particles, and SP-SM, while the fines content varied from 6% to 12% for the SP-SM and from 20% to 34% for the SM (Papathanassiou *et al.*, 2012).

During the same field survey, we also carried out short interviews with the villagers. The information we got is that most of the sandy material within the urban areas of Mirabello, San Carlo and Sant'Agostino was ejected through large diameter water wells starting roughly at the same time of the mainshock. However, in the first seconds/minutes just clear water was outpured and only afterwards it was mixed with silt-sand.

Furthermore, buckling phenomena were locally observed in Mirabello at the base of the levee slope (Figure 6), where contractional features formed due to the differential lateral sliding of building moving downslope on an inclined (even with few degrees) liquefied level (*e.g.* Pizzi and Scisciani, 2012). Similar phenomena have also been documented after the Cephalonia, Greece 2014 (Valkaniotis *et al.*, 2014) and Great East Japan 2011 (*e.g.* Yasuda *et al.*, 2012) earthquakes.

In some cases, when liquefied material during its upward migration encountered a top layer which was resistant enough to impede fracturing but not plastic deformation, say for example a pavement, local bulging structures formed (Figure 7).

As concerns the investigated western sector (*e.g.* Mirandola area), it is noteworthy that though at a similar epicentral distance, only few liquefaction manifestations were reported, including scattered water-sand ejections and liquefaction-induced ground disruptions (Figure 1b). Ground loss due to sand ejecta induced a settlement of about 6 cm in a residential house.

As concerns the liquefaction occurrences that were reported outside of the eastern sector of the meizoseismal zone (Sant'Agostino-San Carlo-Mirabello), Di Manna *et al.* (2012) report that in the area of San Felice sul Panaro the most common and frequently observed effects in urban areas were the ejection of sand from water wells. For example, these effects were mapped (*e.g.* Emergeo WG, 2013) in the area between the stadium and the railway station.

Liquefaction phenomena have also been reported in the Cavezzo village within and near the main canal while few isolated liquefaction surface evidences were mapped around the Medolla village (Emergeo WG, 2013). In addition, liquefaction manifestations were also reported by Di Manna *et al.* (2012) and Emergeo WG (2013) to the northwest of Mirabello and near Scortichino (Obici locality), Burana, San Martino Spino, Bondeno where the dominant type of liquefaction-induced ground disruption was reported to be fractures with sand ejection (Figure 1b).

Quantitative assessment of the liquefaction potential

Data collection

Following the earthquake, a systematic search and collection of all available geognostic information has been carried out in the broader epicentral area by the Servizio Geologico, Sismico e dei Suoli of the Emilia Romagna Region for improving and enriching the already existing database (http://ambiente.regione.emilia-romagna.it/geologia/cartografia/webgis-banchedati/). We contributed to this work particularly for the two areas investigated in this paper. Collected data consist of different typologies from water wells, with or without carrot, to several kinds of penetration tests. For the aims of this paper we considered only piezocone penetration (CPTu), seismic cones (SCPTu) and electrical cone penetration tests (CPTe) in order to maintain the uniformity in our dataset mainly regarding the intervals of measurements. These techniques indeed allow to define with a good accuracy the geotechnical characteristics of the subsoil, say at least the first 20 m, and particularly to calculate the liquefaction potential (*LPI* and *LSN*) at the site.

In order to correlate the numerical results (see following section) with the occurrence or not of liquefaction phenomena in concomitance with the May 20 earthquake, we selected only the test sites for which we have a sure evidence (either positive or negative) of liquefaction-induced ground disruption. Accordingly, we selected 2 CPTe and 47 CPTu and 11 SCPTu most of which have been carried out in the months following the earthquake specifically for seismic microzonation purposes. The selected tests are shown in the maps of Figures 8 and 9, while in Table 1 all relevant information is reported.

For each site, we obtained a simplified stratigraphy of the subsoil based on the interpretation of recorded values of tip resistance and sleeve friction ratio to a soil type behaviour index (Ic) vertical profile. The classification of soil units follows the normalized CPT soil behaviour type chart, proposed by Robertson and Wride (1998) that provides a guide to soil behavior. Therefore, rather than a purely lithological meaning, the obtained units bear a geotechnical information which is a mixture of grain-size distribution and follow generally similar classification of susceptibility to soil liquefaction. In particular, the units referred to as i) sand, ii) sand mixture, iii) silt mixture and iv) clay, correspond to i) clean sand-to-silty sand, ii) silty sand-to-sandy silt, iii) clayey silt-to-silty clay and iv) clay, soils units, respectively.

As concerns the water level depth necessary to calculate the pore pressure profile, the value measured during the drilling was taken into account. All these quantitative analyses were performed using the CLiq software (ver. 1.7.6.34; www.geologismiki.gr).

In Figure 10, are two representative lithostratigraphic profiles for the two investigated areas documenting the lateral variability which characterizes the subsoil from the decameter to the kilometer scale. Indeed, sandy and/or slity sandy layers could vary both in depth from the surface as well as in

thickness, merging with other layers or laterally disappering. Similar geological sections have been presented by Calabrese *et al.* (2012).

Sites specific acceleration

For the quantitative assessment of the liquefaction potential, the ground acceleration at the site represents an important parameter. As far as the two study areas fall within the epicentral zone (*i.e.* near field) where a strong gradient generally occurs due to geometric and anelastic attenuations, it would be not correct to assume a unique acceleration value for all the dataset. Indeed, the distances of the selected sites from the instrumental epicenter fall in the range 10-17 km for the Mirandola area and 12-16 km for the Sant'Agostino area (Figures 1b and 8).

In order to obtain the acceleration value in correspondence of each geotechnical measurement site we considered a ground motion probability equation (GMPE). Among the several such empirical relations proposed in the literature, we selected that proposed by Bindi *et al.* (2011) because i) it is specifically based on the Italian strong motion database ITACA (Luzi *et al.*, 2008; Pacor *et al.*, 2011; http://itaca.mi.ingv.it), ii) it takes into account the style of faulting and iii) it is certainly the most updated one for Italy. The validity of the applied GMPE is in the moment magnitude range 4.0-6.9 and for distances up to 200 km therefore including our dataset parameters.

The PGA estimated with the Bindi *et al.* (2011) GMPE represents the geometrical mean of the two horizontal components. In order to calculate the acceleration at each site, we considered a scalar moment magnitude of 6.1 (Pondrelli *et al.*, 2012) and a hypocentral depth of 7.0 km (Cesca *et al.*, 2013). For estimating the Joyner-Boore distance, R_{JB}, required in the calculation of the GMPE, we applied an empirical relationship between R_{JB} and the epicentral distance (Montaldo *et al.*, 2005). Taking into account that all GMPEs including the one we used (Bindi *et al.*, 2011) assume a radial coseismic rupture and hence a radial distribution of the seismic energy (*viz.* ground acceleration), while the May 20 event was characterized by a strong directivity towards ESE of the rupture propagation (Ganas *et al.*, 2012; Pezzo *et al.*, 2013), for the epicentral location we assumed the vertical projection of the slip plane centroid (Cesca *et al.*, 2013; Ganas *et al.*, 2012; Pezzo *et al.*, 2013), which assured a more realistic distribution of the acceleration especially in the near-field.

According to the information on the shear wave velocity in the first 30 m obtained from the available SCPTUs and following the EC8 (CEN, 2003), all sites were characterized as class C soil (*i.e.* with a v_{s30} in the range 180-360 m/s). The acceleration values for each site calculated on the basis of the Bindi *et al.* (2011)'s GMPE are reported in Table 1 and represented in Figure 11.

The two horizontal accelerations recorded at the Mirandola station (MRN) during the May 20 event, which represents the only available value in the seismic near-field (*i.e.* within a distance comparable to the fault's dimensions), perfectly fit the value we estimated using the Bindi *et al.* (2011) GMPE (Figure 11). Several other stations, though located in the far-field, have recorded PGA values, which mainly fall within the standard deviation curves of the used GMPE for class C.

Evaluating the liquefaction potential

In order to evaluate the liquefaction potential of a soil element, the factor of safety against liquefaction (*Fs*) should be computed using the widely applied stress-based approach, the so called 'simplified procedure', initially proposed by Seed and Idriss (1985) and modified by Youd *et al.* (2001). Nowadays, most of the studies dealing with liquefaction, follow one or more of the approaches proposed by Seed *et al.* (2003), Cetin *et al.* (2004) or Idriss and Boulanger (2008). However, these procedures allow to infer only the behaviour of a single uniform soil layer.

In the present research, for the evaluation of factor of safety, we apply the Idriss and Boulanger (2008) stress-based approach, which compares the earthquake-induced cyclic stress ratio (CSR) with the cyclic resistance ratio of the soil (CRR). Additionally in order to take into account the fines content in the absence of site-specific laboratory test data, we followed the Roberston and Wride (1998) approach. This also allows to maintain the consistency with the procedure followed by Tonkin and Taylor (2013) for the development of *LSN* methodology. As above mentioned, the groundwater level entering the calculation of the factor of safety was recorded during the drilling and listed in Table 1 (meters from the ground surface).

For the computation of the liquefaction potential on the vertical of multiple layers, other approaches should be applied as the one originally proposed by Iwasaki *et al.* (1978; *LPI*) which provides a single value characterizing the performance of the whole soil column. As above mentioned, Tonkin and Taylor (2013) have recently developed a new approach for assessing the type of damaging effects of shallow liquefaction on structures (*LSN*). It is worth mentioning that both methods require numerical information provided by in-situ tests, though the former method (*LPI*) was formulated based on values obtained from SPT, while the latter (*LSN*) by data provided by CPT.

Liquefation Potential Index, LPI

As concerns the *LPI*, the obtained value is proportional to the thickness of the liquefiable layer, to the thickness of the non-liquefiable (cap) layer and to *Fs*

$$LPI = \int_0^h F \cdot w(z)dz \qquad [1]$$

where $F = 1 - Fs$, for $Fs \leq 1$, and $F = 0$, for $Fs > 1$; $w(z) = 10 - 0.5 \cdot z$, with z representing the depth from the surface in meters. The integration depth (h) is commonly limited to 20 m. The parameter *Fs* represents the ratio between CRR and CSR. Iwasaki *et al.* (1978) discriminated some threshold values for the *LPI* based on the severity of liquefaction-induced damages observed during earthquakes and proposed that the liquefaction failure potential should be characterized as 'low' at sites where $0 < LPI < 5$, 'high' where *LPI* is in the range 5-15 and 'very high' above 15.

Sonmez (2003) developed a modified scale by adding a threshold value of 1.2 instead of 1 for the calculation of *Fs* and introduced two new categories of liquefaction failure potential by distinguishing

between 0 and 2 ('non liquefiable') and 2 to 5 ('moderate'). Papathanassiou (2008) proposed an *LPI*-based probabilistic approach for the evaluation of liquefaction-surface evidences and by taking into account a cut-off value of 50% probability he also defined a threshold value of *LPI* = 14 for discriminating the cases of liquefaction manifestation from the non-liquefaction. The above classifications have been developed exclusively using SPT data, while the one proposed by Papathanassiou (2008) took additionally into account the susceptibility to liquefaction criteria proposed by Seed *et al.* (2003) for the classification of the soil layers. Juang *et al.* (2008) suggest that the two threshold values (5 and 15) assumed in the Iwasaki criterion are likely not universally applicable.

An important confirmation of the Iwasaki *et al.* (1978) classification was provided by Toprak and Holzer (2003) which compared *LPI* values with the liquefaction-induced failures of several earthquakes, but obtained from CPTs instead of SPTs. They concluded that sand boils likely occur where $LPI \geq 5$ and lateral spreading phenomena will occur where $LPI \geq 12$. They also suggest that $LPI \geq 5$ can be used as a threshold for the surface manifestation of liquefaction. Furthermore, Lee *et al.* (2004) by applying the Robertson and Wride (1998) method in order to determine the factor of safety, suggest that liquefaction risk is 'high' for sites with $LPI > 21$ and 'low' for sites with $LPI < 13$. Juang *et al.* (2008) computed *LPI* with the concept of probability of surface manifestation of liquefaction (P_G) and recommended the following classification of risk for surface manifestation of liquefaction; 'extremely low' when $P_G < 0.1$, 'low' for $0.1 < P_G < 0.3$, 'medium' when $0.3 < P_G < 0.7$, 'high' when $0.7 < P_G < 0.9$ and 'extremely high' for $P_G > 0.9$. In addition, Juang *et al.* (2008) concluded that the *LPI* scale should be rigorously re-calibrated anytime a component model of the *LPI* procedure is modified, while the discrepancy between the existing calibrations proposed by several authors as briefly reviewed above may be also due to different types of considered liquefiable layers, *e.g.* clear sand or silty sands and sandy silts. For a comprehensive description of the *LPI* and the relevant procedures, the reader is referred to Holzer (2008) and Juang *et al.* (2008).

Liquefation Severity Number, LSN

The *LSN* is a new parameter developed by Tonkin and Taylor (2013) to reflect the more damaging effects of shallow liquefaction and should be considered as a probabilistic measure indicating risk (Tonkin and Taylor, 2013). The *LSN* could be considered as an extension of the philosophy at the basis of the *LPI* and represents an alternative method for assessing the response of structures to liquefaction. The *LSN* rating represents the intensity of liquefaction by using volumetric densification strain as a proxy (e_v), with depth weighting by a hyperbolic (1/z) rather than a linear reduction (van Ballegooy *et al.*, 2012). According to Tonkin and Taylor (2013), the *LSN* is higher for liquefying soils closer to the ground surface in comparison to liquefying layers at depth. The equation that should be used for computing the *LSN* is:

$$LSN = 1000 \cdot \int_0^h \frac{e_v}{z} dz \qquad [2]$$

where the volumetric densification strain in the subject layer, e_v, is estimated by the approach proposed by Zhang *et al.* (2002) and *z* is the depth from the surface to the layer of interest in meters. As in equation [1], the integration depth is commonly posed equal to 20 m because the contribution of the underlying layers would be negligeable.

Based on the observed land damages caused by Christchurch 2010-2011 earthquakes (Tonkin and Taylor, 2010a; 2010b; 2013; Cubrinovski *et al.*, 2011; Orense *et al.*, 2011; Wotherspoon *et al.*, 2012; O'Rourke *et al.*, 2014) and the results provided by thousands CPTs performed in the epicentral area, Tonkin and Taylor (2013) developed a first classification of *LSN* associating 'little-to-no expression of liquefaction' to $0 < LSN < 10$, 'minor expression of liquefaction and sand boils' to $10 < LSN < 20$, 'moderate-to-severe expression of liquefaction and likely settlement' when $20 < LSN < 30$ and 'major expression of liquefaction, damage to ground surface and severe settlement of structures' when $30 < LSN < 40$. Finally for *LSN* values greater than 50, 'severe damage and widespread evidence of liquefaction at the surface' is reported. For a comprehensive description of the *LSN* approach, the reader is referred to Tonkin and Taylor (2013) and van Ballegooy *et al.* (2014).

Comparison between liquefaction potential and observed phenomena

In order to correlate the liquefaction potential to the occurrence or not of liquefaction manifestations triggered by the May 20, 2012 Emilia earthquake, we systematically calculated the *LPI* and *LSN* values for as many as possible *in-situ* tests drilled in the two investigated areas. It should be pointed out that the two epicentral areas, Sant'Agostino and San Carlo, to the east, and Mirandola, to the west, were selected due to the availability of several tests and the fact that the locations of liquefaction manifestations were accurately documented by several post-earthquake field reports (Papathanassiou *et al.*, 2012; Emergeo WG, 2013; Regione Emilia-Romagna, personal communication; UniInsubria, personal communication; Figure 1b).

Although in these reports liquefaction observations are commonly associated with point coordinates, the actual occurrence of the phenomenon at depth is obviously much wider and for this reason we realistically considered liquefaction zones around the observed manifestations following the procedure applied by O'Rourke *et al.* (2014). For the correlation purpose of this paper, all *in-situ* tests falling within these zones were included in the 'liquefied' subset. On the other hand, the identification of 'non-liquefied' areas is a more subtle issue, since it is common during post-earthquake field surveys to emphasize and report mainly the liquefaction occurrences instead of mapping areas without secondary effects. Consequently, for our correlation analysis we selected *in-situ* tests only from areas for which we were absolutely sure that no liquefaction phenomena were triggered by the May 20 earthquake. In so doing, if the number of sites statistically analyzed was reduced compared to the *in-*

situ tests available for the two epicentral areas, the reliability and the accuracy of the results have certainly benefitted. Tests drilled within 'liquefied' and 'not-liquefied' zones are indicated in Table 1.

In summary, a total of 60 in-situ tests were selected (23 and 37 in the western and eastern study areas, respectively) of which 23 drilled in 'liquefied' zones and 37 in 'non-liquefied' zones (Table 1). In Figures 8 and 9, are represented the maps of the two investigated areas with the obtained *LPI* and *LSN* values, respectively, as well as the liquefied zones.

For the 'liquefied' zones, the values of the *LPI* range from 6.9 to 27.6 and the values of the *LSN* from 7.5 to 25.7 (Table 1). In contrast, for the 'non-liquefied' zones the values are commonly smaller than 10 for both *LPI* and *LSN*, with only few exceptions.

As above mentioned, the obtained values of the *LSN* have been separated in two subsets based on their correlation with liquefied or not-liquefied zones as observed in the field after the earthquake. Their statistical distribution is graphically shown in Figure 12. Although the present research represents the first attempt after the Christchurch case study of applying the *LSN* methodology and correlating the calculated values to the occurrences of liquefaction, our results are in good agreement with the classification proposed by Tonkin and Taylor (2013), which propose a threshold value of 10. Indeed, in the liquefied and non-liquefied subsets the 77.3% and 83.3% of the data have a value respectively greater or smaller than the threshold of 10 (Figure 12).

As concerns the statistical distribution of the *LPI* (Figure 12), several threshold values have been proposed in the literature for separating potentially liquefiable conditions from not liquefiable ones. For example, the value of 5 as proposed by Iwasaki et al. (1978), Toprak and Holzer (2003) and Sonmez (2003), clearly does not justify our results as far as 36.2% of the non-liquefied sites have an *LPI* value greater than 5. In contrast, if we assume a threshold of *LPI* = 13 or 14 as proposed by Lee *et al.* (2004) and Papathanassiou (2008), respectively, almost all non-liquefied sites are characterized by smaller calculated values (97.3%). Moreover, 86.4% and 72.8%, of the *in-situ* tests drilled where liquefaction was triggered provides an *LPI* value which is higher than the threshold of Lee *et al.* (2004) and Papathanassiou (2008), respectively.

Concluding remarks

The 20th May, 2012 earthquake that occurred in Emilia Romagna, northern Italy triggered widespread liquefaction phenomena in the epicentral area. The most impressive liquefaction surface evidences were documented in a zone including the urban areas of Sant'Agostino, San Carlo and Mirabello. Few weeks after the event, several boreholes with *in-situ* tests were drilled in the epicentral area providing crucial information regarding the geotechnical characteristics of the subsoil layers. This information has been systematically collected and analyzed in order to evaluate the liquefaction potential in these sites by computing the *LPI* and *LSN* values.

Initially, the liquefaction potential of the soil layers encountered in these boreholes, defined as

factor of safety, was evaluated using the Idriss and Boulanger (2008) simplified procedure, while the estimation of fines content was achieved by applying Robertson and Wride (1998) method. Afterwards, since reliable and accurate field observations of liquefaction-induced failures exist and data provided by CPTu and SCPTu are available, the outcome of the evaluation of liquefaction potential parameters, *e.g. LPI* and *LSN*, has been correlated to the occurrence or not of liquefaction and compared with the existing relevant classifications. It is thus believed that the outcome of this comparison could provide a useful feedback regarding the *LPI* and, for the first time, of the *LSN* approaches.

From the comparison, we conclude that the computed *LSN* values are in agreement with the proposed classification of Tonkin and Taylor (2013). In particular, regarding the liquefied sites, it was found that most of the *LSN* values are higher than 10 (77.3%), the threshold between the little-to-no expression of liquefaction and minor expression of liquefaction. Even more robust from a statistical point of view is the percentage of tests drilled in no-liquefied zones and characterized by $LSN < 10$ (83.3%).

However, taking into account the amount of ejecta observed, it would be expected that the *LSN* values in liquefied zones should be higher. This apparent discrepancy may be explained by the fact that the upward moving of liquefied sandy material was facilitated by the presence of wells in almost every courtyard of San Carlo (Figure 3). Without the existence of these wells it is not sure that the same amount of sandy material would have been able to penetrate the crust layer and reach the surface.

Another possible cause of the large number of liquefaction occurrences in the eastern investigated area of San Carlo-Sant'Agostino, could be correlated to the fact that the potentially liquefiable sandy bodies in the first 5-30 m-depth generally represent semiconfined-to-confined acquifers (Figure 10). It is noteworthy that within the broader epicentral area, some boreholes equipped with probes for water level monitoring (sampling frequency of 1 hour), have recorded an abrupt increase of the piezometric surface up to 1.6 m. Two of the boreholes (Fe-80 and Fe-81) exploit both the semi-confined (*A0*) and the first confined (*A1*) acquifer systems, while the well Mo-80 only acquifer *A1* (see Figure 1b for wells location). Considering the exponential decay of the water level back to 'normal' conditions, the epicentral distance of the instrumented boreholes and the fact that the first measurement was carried out 'only' 57 minutes after the main shock (Marcaccio and Martinelli, 2012; ARPA-RER database, Marcaccio M. personal communication), it is reasonable to assume a much greater co-seismic piezometric anomaly within the meizoseismal area. A strong transient overpressure is also supported by our field observations and several original witnesses. For example, in San Carlo (44°48'15.39"N, 11°24'35.14"E) a water-sand mixture was ejected up to 2 m above ground surface (Caputo and Papathanassiou, 2012). Taking into account that local water depth before the earthquake was approximately 6 m and the ejected material density is obviously greater than water, a rough overpressure of about 1 bar (0.1 MPa) could be estimated.

It is worth to recall that regarding the pore pressure, which is a parameter included in the calculation of both *LPI* and *LSN* values, we followed the standard procedure by assuming the values measured during the drilling, that is when the water pressure was in 'normal' interseismic conditions. As a consequence, the hydraulic anomaly generated in the shallow sandy bodies during the May 20 shaking has been not included in our calculations, but it has certainly influenced the geotechnical behaviour of the drilled sites by enhancing the liquefaction process and hence the distribution of sand-water mixture surface ejections.

Another issue that arises is that the *LSN* classification has been formulated using the Robertson and Wride (1998) approach for the estimation of fines content, an approach that has been characterized as not conservative by Idriss and Boulanger (2008). Therefore, the proposed boundaries of the classes should be further investigated by applying approaches that include the fines content directly obtained from laboratory tests (*e.g.* Idriss and Boulanger, 2008).

The correlation of the computed *LPI* values with the existing classifications of Iwasaki *et al.* (1978), Sonmez (2003) and Toprak and Holzer (2003) are not in agreement since 36% of non-liquefied sites had *LPI* values higher than 5, a value that have been used as the threshold for the very unlikely or low risk liquefaction sites. However, this outcome is in agreement with *LPI* classifications and the relevant threshold values proposed by Lee *et al.* (2004) and Papathanassiou (2008) (13 and 14, respectively) as far as 97% of non-liquefied sites are characterized by smaller calculated values, while 86.4% and 72.8% (respectively for the two threshold values) of the *in-situ* tests drilled within the liquefied zones have higher *LPI* values.

As a final comment, the present research and our results show that the use of both *LPI* and *LSN* could likely improve the outcomes of microzonation studies allowing to better characterise the liquefaction hazard of urban areas.

Acknowledgements

We thank Pavlides S. and Chatzipetros A. (AUTh) for discussions, Martelli L. (Geological Survey RER) and Marcaccio M. (ARPA-RER) for providing several geotechnical, hydrological and field data and Ioannides J. (GeoLogismiki) for providing the Academic license of the CLiq software. P.G. also thanks the AUTh for permission to temporary work at the University of Ferrara and the co-financing received from the European Social Fund (ESF) and the Greek Operational Program "Education and Lifelong Learning" of the National Strategic Reference Framework (NSRF) and Program Thales ("Investing in knowledge society through the European Social Fund", Project 85330 - Characterization of site conditions in Greece for realistic seismic ground motion simulations: pilot application in urban areas).

References

Bartolini C., Caputo R. and Pieri M. (1996): Pliocene-Quaternary sedimentation in the Northern Apennine Foredeep and related denudation. *Geol. Magazine*, **133**(3), 255-273.

Basili R., Valensise G., Vannoli P., Burrato P., Fracassi U., Mariano S., Tiberti M.M. and Boschi E. (2008): The Database of Individual Seismogenic Sources (DISS), version 3: summarizing 20 years of research on Italy's earthquake geology. *Tectonophys.*, **453**(1-4), 20-43 doi:10.1016/j.tecto.2007.04.014

Bigi G., Bonardini G., Catalano R., Cosentino D., Lentini F., Parlotto M. Sartori R., Scandone P. and Turco E. (1992): *Structural model of Italy, 1:500,000*. Consiglio Nazionale delle Ricerche, Rome.

Bignami C., Burrato P., Cannelli V., Chini M., Falcucci E., Ferretti A., Gori S., Kyriakopoulos C., Melini D., Moro M., Novali F., Saroli M., Stramondo S., Valensise G. and Vannoli P. (2012): Coseismic deformation pattern of the Emilia 2012 seismic sequence imaged by Radarsat-1 interferometry. *Annals of Geophys.*, **55**(4), 788-795, doi: 10.4401/ag-6157.

Bindi D., Pacor F., Luzi L., Puglia R., Massa M., Ameri G. and Paolucci R. (2011): Ground motion prediction equations derived from the Italian strong motion database. *Bull. Earthquake Eng.*, **9**, 1899-1930, doi: 10.1007/s10158-011-9313-z.

Boccaletti M., Bonini M., Corti G., Gasperini P., Martelli L., Piccardi L., Tanini C. and Vannucci G. (2004): *Seismotectonic Map of the Emilia-Romagna Region, 1:250000*. Regione Emilia-Romagna – CNR.

Bondesan M. (1989): *Evoluzione geomorfologica e idrografica della pianura ferrarese*. Terre ed acqua, Corbo Editore, 14-20.

Bonini L., Toscani G. and Seno S. (2014): Three- dimensional segmentation and different rupture behavior during the 2012 Emilia seismic sequence (Northern Italy). *Tectonophys.*, **2014**, TECTO-126307 (in press).

Bozzoni F., Lai C.G. and Scandella L. (2012): Preliminary results of ground-motion characteristics. *Ann. Geophys.*, **55**(4), 609-614, doi: 10.4401/ag-6121.

Bray J., Cubrinovski M., Zupan J. and Taylor M. (2014): Liquefaction Effects on Buildings in the Central Business District of Christchurch. *Earthquake Spectra*, **30**(1), 85-109, doi: http://dx.doi.org/10.1193/022113EQS043M.

Burrato P., Ciucci F. and Valensise G. (2003): An inventory of river anomalies in the Po Plain, northern Italy: evidence for active blind thrust faulting. *Annals of Geophys.*, **46**(5), 865-882.

Burrato P., Vannoli P., Fracassi U., Basili R. and Valensise G. (2012): Is blind faulting truly invisible? Tectonic-controlled drainage evolution in the epicentral area of the May 2012, Emilia-Romagna earthquake sequence (northern Italy). *Annals of Geophys.*, **55**(4), 525-531, doi: 10.4401/ag-6182.

Calabrese L., Martelli L. and Severi P (2012): Stratigrafia dell'area interessata dai fenomeni di liquefazione durante il terremoto dell'Emilia (maggio 2012). 31° Conv. Naz. GNGTS, Potenza, November 20-22, 2012, *Atti*, **2**, 119-126.

Caputo R. (2005): Ground effects of large morphogenic earthquakes. *J. Geodyn.*, **40**(2-3), 113-118.

Caputo R. and Papathanasiou G. (2012): Ground failure and liquefaction phenomena triggered by the 20 May, 2012 Emilia-Romagna (Northern Italy) earthquake: case study of Sant'Agostino - San Carlo - Mirabello zone. *Nat. Haz. Earth System Sciences*, **12**(11), 3177-3180, doi:10.5194/nhess-12-3177-2012.

Caputo R., Iordanidou K., Minarelli L., Papathanassiou G., Poli M.E., Rapti-Caputo D., Sboras S., Stefani M. and Zanferrari A. (2012a): Geological evidence of pre-2012 seismic events, Emilia-Romagna, Italy. *Ann. Geophysics*, **55**(4), 743-749, doi: 10.4401/ag-6148.

Caputo R., Iordanidou K., Minarelli L., Papathanassiou G., Poli M.E., Rapti-Caputo D., Sboras S., Stefani M. and Zanferrari A. (2012b): Paleoliquefazioni nell'area epicentrale del terremoto emiliano del 2012. 31° Convegno Nazionale GNGTS, Potenza, November 20-22, 2012, *Atti*, **2**, 14-20; ISBN 978-88-90101-2-9

CEN (Comité Européen de Normalisation) (2003): *prEN 1998-1- Eurocode 8: design of structures for earthquake resistance. Part 1: General rules, seismic actions and rules for buildings*. Draft No 6, Doc CEN/TC250/SC8/N335, January 2003, Brussels.

Cesca S., Braun T., Maccaferri F., Passarelli L., Rivalta E. and Dahm T. (2013): Source modelling of the M5–6 Emilia-Romagna, Italy, earthquakes (2012 May 20–29). *Geophys. J. Int.*, **193**(3): 1658-1672, doi:10.1093/gji/ggt069.

Cetin K.O., Seed R.B., Kiureghian A.D., Tokimatsu K., Harder Jr. L.F., Kayen R.E. and Moss R.E.S. (2004): Standard penetration testbased probabilistic and deterministic assessment of seismic soil liquefaction potential. J. Geotech. Geoenviron. Eng., **130**(12), 1314-1340.

C.N.R. (1992): *Structural Model of Italy*. Prog. Fin. Geodinamica, sottoprog. Modello strutturale tridimensionale.

Cubrinovski M., Bray J.D., Taylor M., Giorgini S., Bradley B., Wotherspoon L., and Zupan J. (2011): Soil Liquefaction Effects in the Central Business District during the February 2011 Christchurch Earthquake. *Seismol. Res. Lett.*, **82**(6), 893-904, doi:10.1785/gssrl.82.6.893.

Di Manna P., Guerrieri L., Piccardi L., Vittori E., Castaldini D., Berlusconi A., Bonadeo L., Comerci V., Ferrario F., Gambillara R., Livio F., Lucarini M. and Michetti A.M. (2012): Ground effects induced by the 2012 seismic sequence in Emilia: implications for seismic hazard assessment in the Po Plain. *Ann. Geophys.*, **55**(4), 697-703.

DISS Working Group (2010). Database of Individual Seismogenic Sources (DISS), Version 3.1.1: A compilation of potential sources for earthquakes larger than M 5.5 in Italy and surrounding areas. http://diss.rm.ingv.it/diss/, © INGV 2010 - Istituto Nazionale di Geofisica e Vulcanologia - All rights reserved; doi:10.6092/INGV.IT-DISS3.1.1

Emergeo Working Group (2013): Liquefaction phenomena associated with the Emilia earthquake sequence of May–June 2012 (Northern Italy). *Nat. Haz. Earth Syst. Sci.*, **13**, 935-947

Galli P., Castenetto S. and Peronace E. (2012): May 2012 Emilia earthquakes (Mw 6, Norterhn Italy): macroseismic effects distribution and seismotectonic implications. *Alpine and Mediterranean Quaternary*, **25**(2), 105-123.

Ganas A., Roumelioti Z., and Chousianitis K. (2012): Static stress transfer from the May 20, 2012, M 6.1 Emilia-Romagna (northern Italy) earthquake using a co-seismic slip distribution model. *Ann. Geophys.*, **55**(4). doi:10.4401/ag-6176

Ghielmi M., Minervini M., Nini C., Rogledi S., Rossi M. and Vignolo A. (2010): Sedimentary and tectonic evolution in the eastern Po-Plain and northern Adriatic Sea area from Messinian to Middle Pleistocene (Italy). *Rend. Fis. Acc. Lincei*, **21**, Suppl. 1, S131-S166, doi: 10.1007/s12210-010-0101-5.

Holzer T.L. (2008): Probabilistic liquefaction hazard mapping. In Zeng D., Manzari M.T. and Hiltunen D. (eds.), Geotechnical Earthquake Engineering and Soil Dynamics Conference, 4th, Sacramento, Proceedings, ASCE Geotechnical Special Publication No. 181, p. 1-32.

Idriss I.M. and Boulanger R.W. (2008): *Soil liquefaction during earthquakes*. MNO–12, Earthquake Engineering Research Institute, 242 pp., Oakland, USA.

Iwasaki T., Tatsuoka F., Tokia K.i. and Yasuda S. (1978): A practical method for assessing soil liquefaction potential based on case studies at various sites in Japan. 2nd Int. Conf. on Microzonation, San Francisco, *Proceedings*, 885-896.

Juang C. Hsein, Liu Chia-Nan, Chen Chien-Hsun, Hwang Jin-Hung, Lu Chih-Chieh (2008). Calibration of liquefaction potential index: A re-visit focusing on a new CPTU model, *Eng. Geol*.. **102**, 19-30

Lee, D.H., Ku, C.S., Yuan, H., 2004. A study of the liquefaction risk potential at Yuanlin, Taiwan. *Eng. Geol.*, **71**, 97–117.

Luzi L., Hailemikael S., Bindi D., Pacor F., Mele F. and Sabetta F. (2008): ITACA (ITalian ACcelerometric Archive): a web portal for the dissemination of Italian strong motion data. *Seismol. Res. Lett.*, **79**(5), 716-722, doi:10.1785/gssrl.79.5.716

Massa M., Augliera P., Carannante S., Cattaneo M., D'Alema E., Lovati S., Monachesi G., Moretti M. and Piccinini D. (2013): D18/b2 – Relocated seismicity in the Po Plain. DPC-INGV-S1 Project, *Final Report*, 213-222.

Michetti A.M., Esposito E., Guerrieri L., Porfido S., Serva L., Tatevossian R., Vittori E., Audemard F., Azuma T., Clague J., Comerci V., Gurpinar A., McCalpin J., Mohammadioun B., Morner N.A., Ota Y. and Roghozin E. (2007): Intensity Scale ESI 2007. In: Guerrieri L. and Vittori E. (Eds), *Memorie Descrittive Carta Geologica d'Italia*, APAT, Servizio Geologico d'Italia— Dipartimento Difesa del Suolo, Roma, Italy, **74**, 53 pp.

Molinari F.C, Boldrini G., Severi P., Duroni G., Rapti-Caputo D. and Martinelli G. (2007): *Risorse idriche sotterranee della Provincia di Ferrar*a. Regione Emilia Romagna, DB MAP Ed. (Florence), pp. 61.

Montaldo V., Faccioli E., Zonno G., Akinci A. and Malagnini L. (2005): Treatment of ground-motion predictive relationships for the reference seismic hazard map of Italy. *J. Seismol.*, **9**(3), 295-316, doi: 10.1007/s10950-005-5966-x.

M.U.R.S.T. (1997): *Carta Geomorfologica della Pianura Padana alla scala 1:250.000.* coord. Castiglioni G.B., S.EL.CA., Firenze.

Orense R.P., Kiyota T., Yamada S., Cubrinovski M., Hosono Y., Okamura M. and Yasuda S. (2011): Comparison of liquefaction Features observed during the 2010 and 2011 Canterbury earthquakes. *Seismol. Res. Lett.*, **82**(6), 905-918, doi:10.1785/gssrl.82.6.905.

O'Rourke T.D., Jeon S.-S., Toprak S., Cubrinovski M., Hughes M., van Ballegooy S. and Bouziou D. (2014): Earthquake Response of Underground Pipeline Networks in Christchurch, NZ. *Earthq. Spectra*, **30**(1), 183-204, doi: 10.1193/030413EQS062M.

Pacor F., Paolucci R., Ameri G., Massa M. and Puglia R. (2011): Italian strong motion records in ITACA: overview and record processing. *Bull. Earth. Eng.*, **9**(6), 1741-1759, doi: 10.1007/s10518-011-9295-x.

Papathanassiou, G. (2008). LPI-based approach for calibrating the severity of liquefaction- induced failures and for assessing the probability of liquefaction surface evidence. *Eng. Geol.*, **96**, 94-104.

Papathanassiou G., Caputo R. and Rapti-Caputo D. (2012): Liquefaction phenomena along the palaeo-Reno River caused by the May 20, 2012 Emilia (Northern Italy) earthquake. *Ann. Geophys.*, **55**(4), 735-742, doi: 10.4401/ag-6147.

Pezzo G., Merryman Boncori J.P., Tolomei C., Salvi S., Atzori S., Antonioli A., Trasatti E., Novali F., Serpelloni E., Candela L. and Giuliani R. (2013): Coseismic Deformation and Source Modeling of the May 2012 Emilia (Northern Italy) Earthquakes. *Seism. Res. Letts.*, **84**(4), 645-655, doi: 10.1785/0220120171.

Pieri M. and Groppi G. (1981): *Subsurface geological structure of the Po Plain, Italy*. Consiglio Nazionale delle Ricerche, Progetto finalizzato Geodinamica, sottoprogetto Modello Strutturale, pubbl. N° 414, Roma, 13 pp.

Pizzi A. and Scisciani V. (2012): The May 2012 Emilia (Italy) earthquakes: preliminary interpretations on the seismogenic source and the origin of the coseismic ground effects. *Ann. Geophys.*, **55**(4), 751-757, doi: 10.4401/ag-6171.

Pondrelli S., Salimbeni S., Perfetti P. and Danecek P. (2012): Quick regional centroid moment tensor solutions for the Emilia 2012 (northern Italy) seismic sequence. *Ann. Geophys.*, **55**(4), 615-621, doi: 10.4401/ag-6146.

Rapti-Caputo D. and Martinelli G. (2009): Geochemical and isotopic composition of the groundwater resources of the Po River delta (Northern Italy): implications for the environmental impact. *J. Hydrogeology*, **17**, 467-480.

Robertson P.K. (1990): Soil classification using the cone penetration test. *Canadian Geotechnical Journal*, **27**(1), 151-158.

Robertson P.K. and Wride C.E. (1998): Evaluating cyclic liquefaction potential using the cone penetration test. *Canadian Geotechnical Journal*, **35**, 442-459.

Salvi S., Tolomei C., Merryman Boncori J.P., Pezzo G., Atzori S., Antonioli A., Trasatti E., Giuliani R., Zoffoli S. and Coletta A. (2012): Activation of the SIGRIS monitoring system for ground deformation mapping during the Emilia 2012 seismic sequence, using COSMO-SkyMed InSAR data. *Ann. Geophys.*, **55**(4), 796-802, doi: 10.4401/ag-6181.

Seed H.B., Tokimatsu K., Harder L.F. and Chung R.M. (1985): The influence of SPT procedures in soil liquefaction resistance evaluations. *J. Geotech. Eng.* Division, ASCE, **111**(12), 1425-1445.

Seed R.B., Cetin K.O., Moss R.E.S., Kammerer A.M., Wu J., Pestana J.M., Riemer M.F., Sancio R.B., Bray J.D., Kayen R.E. and Faris A. (2003): Recent advances in soil liquefaction engineering: a unified and consistent framework. 26th annual ASCE L.A. Geotechnical Spring Seminar, Long Beach, California. 71 pp.

Sonmez, H. (2003): Modification of the liquefaction potential index and liquefaction susceptibility mapping for a liquefaction-prone area (Inegol, Turkey). *Environmental Geology* **44**(7), 862-871.

Tonkin and Taylor (2010a): *Darfield Earthquake 4 September 2010 Geotechnical Land Damage Assessment & Reinstatement. Stage 1 Report*. 38 pp., Earthquake Commission (http://www.tonkin.co.nz/canterbury-land-information/docs/T&T-Stage%201%20Report.pdf, last visited May 9, 2014).

Tonkin and Taylor (2010b): *Darfield Earthquake 4 September 2010 Geotechnical Land Damage Assessment & Reinstatement. Stage 2 Report*. 72 pp., Earthquake Commission (http://www.tonkin.co.nz/canterbury-land-information/docs/T&T-Stage%202%20Report.pdf, last visited May 9, 2014).

Tonkin and Taylor (2013): *Canterbury Earthquakes 2010 and 2011. Land report as at 29 February 2012*. 108 pp., Earthquake Commission (http://www.tonkin.co.nz/canterbury-land-information/docs/downloads2592013/T&T-Stage-3-Report.pdf, last visited May 9, 2014).

Toprak S., and Holzer T.L. (2003): Liquefaction Potential Index: Field Assessment. *J. Geotech. Geoenviron. Eng.*, **129**(4), 315-322.

Tsuchida H. (1971): Estimation of liquefaction potential of sandy soils. 3rd Joint Meeting US-Japan Panel on Wind and Seismic Effects, UJNR, *Proceedings*.

Valkaniotis S., Ganas A., Papathanasiou G., Papanikolaou M (2014): Field observations of geological effects triggered by the January–February 2014 Cephalonia (Ionian Sea, Greece) earthquakes. *Tectonophys.*, doi: 10.1016/j.tecto.2014.05.012

van Ballegooy S., Malan P., Lacrosse V., Jacka M.E., Cubrinovski M., Bray J.D., O'Rourke T.D., Crawford S.A. and Cowan H. (2014): Assessment of Liquefaction-Induced Land Damage for Residential Christchurch. *Earthquake Spectra*, **30**(1), 31-55, doi: http://dx.doi.org/10.1193/031813EQS070M.

Wotherspoon L.M., Pender M.J. and Orense R.P. (2012): Relationship between observed liquefaction at Kaiapoi following the 2010 Darfield earthquake and former channels of the Waimakariri River. *Eng. Geol.*, **125**, 45-55, doi:10.1016/j.enggeo.2011.11.001.

Yasuda S., Harada K., Ishikawa K. and Kanemaru Y. (2012): Characteristics of liquefaction in Tokyo Bay area by the 2011 Great East Japan Earthquake. *Soils and Foundations*, 52(5), 793–810.

Youd T.L., Idriss I.M., Andrus R.D., Arango I., Christian J.T., Dobry R., Finn W.D.L., Harder L.F., Hynes M.E., Ishihara K., Koester J.P., Liao S.S.C., Marcuson W.F., Martin G. R., Mitchell J.K., Moriwaki Y., Power M.S., Robertson P.K., Seed R.B. and Stokoe K.H. (2001): Liquefaction Resistance of Soils: Summary Report from the 1996 NCEER and 1998 NCEER/NSF Workshops on Evaluation of Liquefaction Resistance of Soils. *J. Geotech. Geoenviron. Eng.*,127(10), 817-833.

Zhang G., Robertson P.K. and Brachman R. (2002): Estimating Liquefaction Induced Ground Settlements from the CPT, *Canad. Geotech. J.*, **39**, 1168-1180.

Table

Click here to download Table: table1.docx

n	RER code	latitude	longitude	water table	PGA	liquefied zone	*LPI*	*LSN*
1	184090U053	44°52'02"	11°00'03"	4.90	0.19	N	0.2	0.0
2	184090U054	44°52'01"	11°00'03"	4.90	0.19	N	0.3	0.0
3	184090U055	44°51'35"	11°02'08"	3.40	0.23	N	1.2	0.6
4	184050U015	44°54'12"	11°02'38"	4.20	0.22	N	1.3	0.3
5	184050U016	44°54'13"	11°02'38"	4.20	0.22	N	2.7	1.5
6	184050U017	44°54'54"	11°02'39"	2.65	0.22	N	1.6	1.2
7	184050U018	44°54'54"	11°02'39"	3.45	0.22	N	2.4	1.5
8	184090B003	44°53'19"	11°03'19"	4.45	0.25	N	3.3	0.8
9	184090U052	44°53'55"	11°03'45"	2.50	0.25	N	4.9	2.3
10	184090U051	44°53'55"	11°03'47"	2.50	0.25	N	5.5	3.3
11	184090U046	44°53'39"	11°03'59"	4.30	0.26	N	5.5	0.4
12	184010E002	44°57'05"	11°04'02"	2.20	0.21	N	0.8	0.6
13	184010E001	44°57'06"	11°04'02"	2.20	0.21	N	1.0	0.5
14	184090U050	44°53'30"	11°04'14"	3.20	0.27	N	2.0	1.6
15	184090U049	44°53'31"	11°04'14"	3.25	0.27	N	2.4	1.4
16	184090U047	44°53'30"	11°04'15"	4.20	0.27	N	5.2	3.2
17	184090U048	44°53'30"	11°04'15"	3.70	0.27	N	6.3	3.2
18	184090B004	44°52'47"	11°04'44"	5.72	0.29	N	1.7	0.2
19	MI_01	44°57'33"	11°05'18"	1.00	0.22	N	16.1	4.8
20	CPTU2	44°53'47"	11°05'44"	1.40	0.31	Y	25.7	20.7
21	CPTU1	44°53'47"	11°05'46"	1.40	0.31	Y	18.9	14.4
22	MI_02	44°53'36"	11°06'44"	1.00	0.34	N	6.4	9.7
23	184060U001	44°54'14"	11°06'51"	3.80	0.31	N	10.6	5.5
24	203010U509	44°47'06"	11°21'06"	1.90	0.72	N	13.3	8.7
25	203010U013	44°47'30"	11°22'26"	2.00	0.69	N	18.9	11.7
26	203010U009	44°47'33"	11°22'29"	1.00	0.69	N	20.0	11.5
27	185130U006	44°48'52"	11°22'47"	3.00	0.73	N	1.5	2.1
28	203010U005	44°47'20"	11°22'47"	2.40	0.66	Y	19.1	9.6
29	203010U006	44°47'18"	11°22'49"	2.40	0.65	Y	12.6	7.5
30	203010U001	44°47'37"	11°23'16"	4.00	0.65	Y	13.9	16.9
31	203010U002	44°47'40"	11°23'16"	4.90	0.65	Y	15.5	17.1
32	185130U505	44°48'13"	11°24'25"	5.00	0.60	Y	9.0	12.2
33	185130U506	44°48'16"	11°24'29"	4.84	0.60	Y	16.6	18.1
34	185130B502	44°48'20"	11°24'29"	3.00	0.60	Y	25.4	25.7
35	185130B995	44°48'15"	11°24'31"	2.00	0.60	Y	8.4	15.1
36	185130U507	44°48'16"	11°24'32"	5.16	0.60	Y	13.5	15.2
37	185130B501	44°48'13"	11°24'33"	3.00	0.59	Y	15.6	15.9
38	185130U509	44°48'20"	11°24'36"	2.37	0.59	N	4.6	8.9
39	185130U508	44°48'17"	11°24'36"	4.22	0.59	Y	8.2	11.2
40	185130B503	44°48'18"	11°24'36"	3.00	0.59	Y	27.6	25.7
41	185130B996	44°48'13"	11°24'37"	1.40	0.59	Y	19.5	16.6
42	185130U510	44°48'21"	11°24'41"	5.23	0.59	N	6.0	8.6

43	185130B504	44°48'27"	11°24'43"	3.00	0.59	Y	25.8	23.4
44	185130U511	44°48'23"	11°24'44"	4.65	0.59	N	6.6	8.8
45	185130U512	44°48'25"	11°24'50"	4.40	0.58	Y	9.7	13.6
46	185130B999	44°48'25"	11°24'51"	5.40	0.58	Y	11.9	15.2
47	185130U513	44°48'26"	11°24'52"	4.18	0.58	Y	20.3	21.0
48	185130B998	44°48'26"	11°24'53"	4.00	0.58	Y	14.7	19.7
49	185130U514	44°48'26"	11°24'56"	4.55	0.58	Y	19.7	20.3
50	185130U022	44°48'40"	11°24'58"	1.80	0.58	N	10.7	7.0
51	185140U005	44°48'31"	11°25'15"	4.90	0.56	N	0.0	0.0
52	185140B001	44°48'17"	11°25'24"	2.00	0.54	N	8.9	16.5
53	185140U003	44°48'19"	11°25'27"	3.60	0.54	N	0.8	0.9
54	185140U004	44°48'20"	11°25'29"	3.30	0.54	N	0.2	0.8
55	185140U002	44°48'08"	11°25'35"	2.30	0.53	N	9.9	7.8
56	203020U099	44°47'51"	11°25'47"	1.80	0.51	N	7.9	6.9
57	203020U098	44°47'52"	11°25'50"	1.90	0.50	N	0.6	1.7
58	203020U097	44°47'54"	11°25'54"	2.05	0.50	N	4.6	10.5
59	203020U096	44°47'57"	11°26'13"	1.60	0.48	Y	6.9	13.9
60	203020U095	44°47'58"	11°26'13"	4.50	0.48	Y	9.0	13.6

LPI and *LSN* values calculated for the test sites (last two columns). The number in the first column is used in Figure 12, while the test code in the database of the Regione Emilia-Romagna (http://ambiente.regione.emilia-romagna.it/geologia/cartografia/webgis-banchedati/) is reported in the second column. Water table is in meters below ground surface. Peak ground acceleration (PGA) as percentage of gravity (see text for discussion). Test sites drilled within liquefied (Y) and not-liquefied (N) zones are indicated.

Figure

Click here to download high resolution image

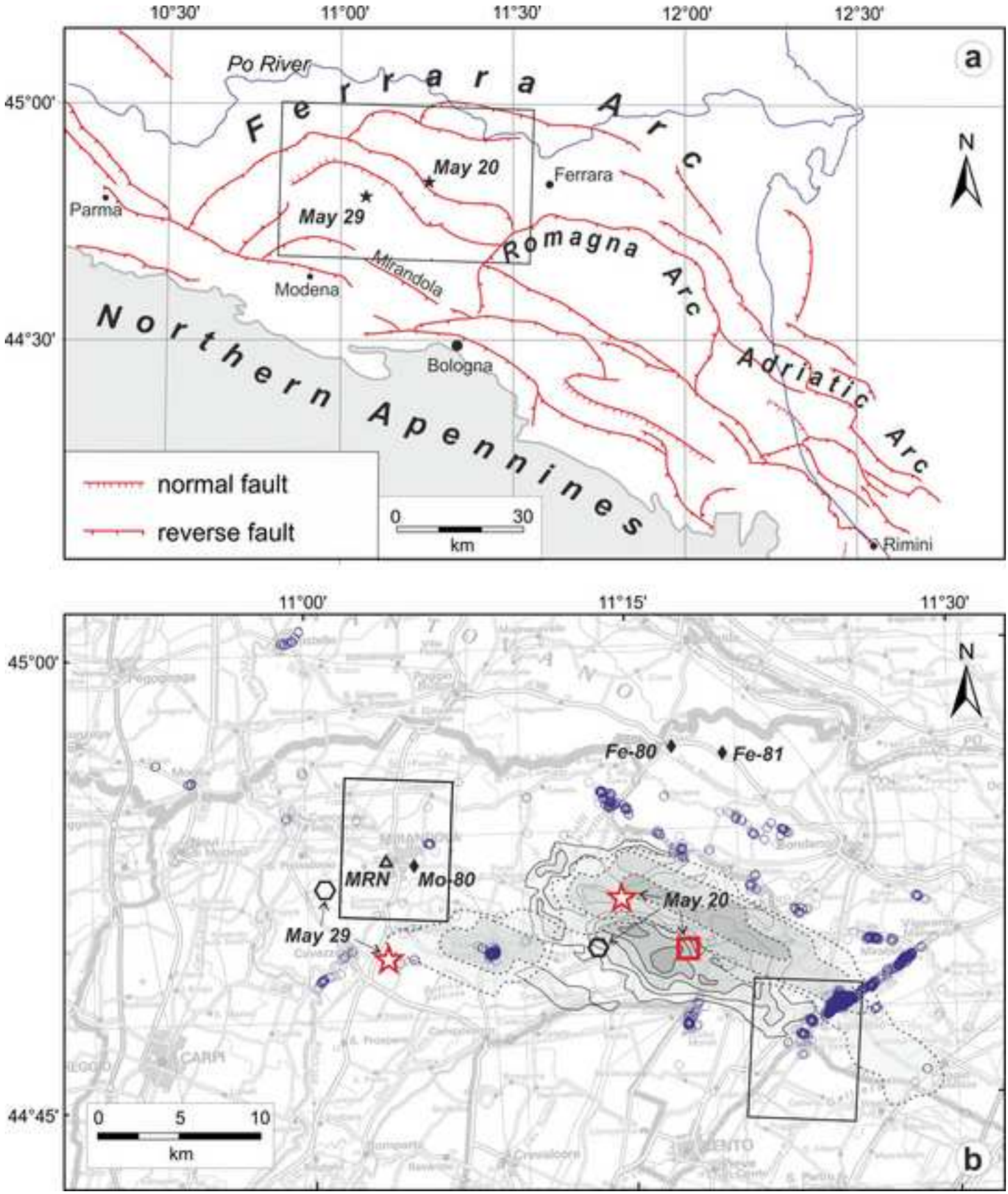

Figure

Click here to download high resolution image

Figure

Click here to download high resolution image

Figure
Click here to download high resolution image

Figure

Click here to download high resolution image

Figure

Click here to download high resolution image

Figure

Click here to download high resolution image

Figure

Click here to download high resolution image

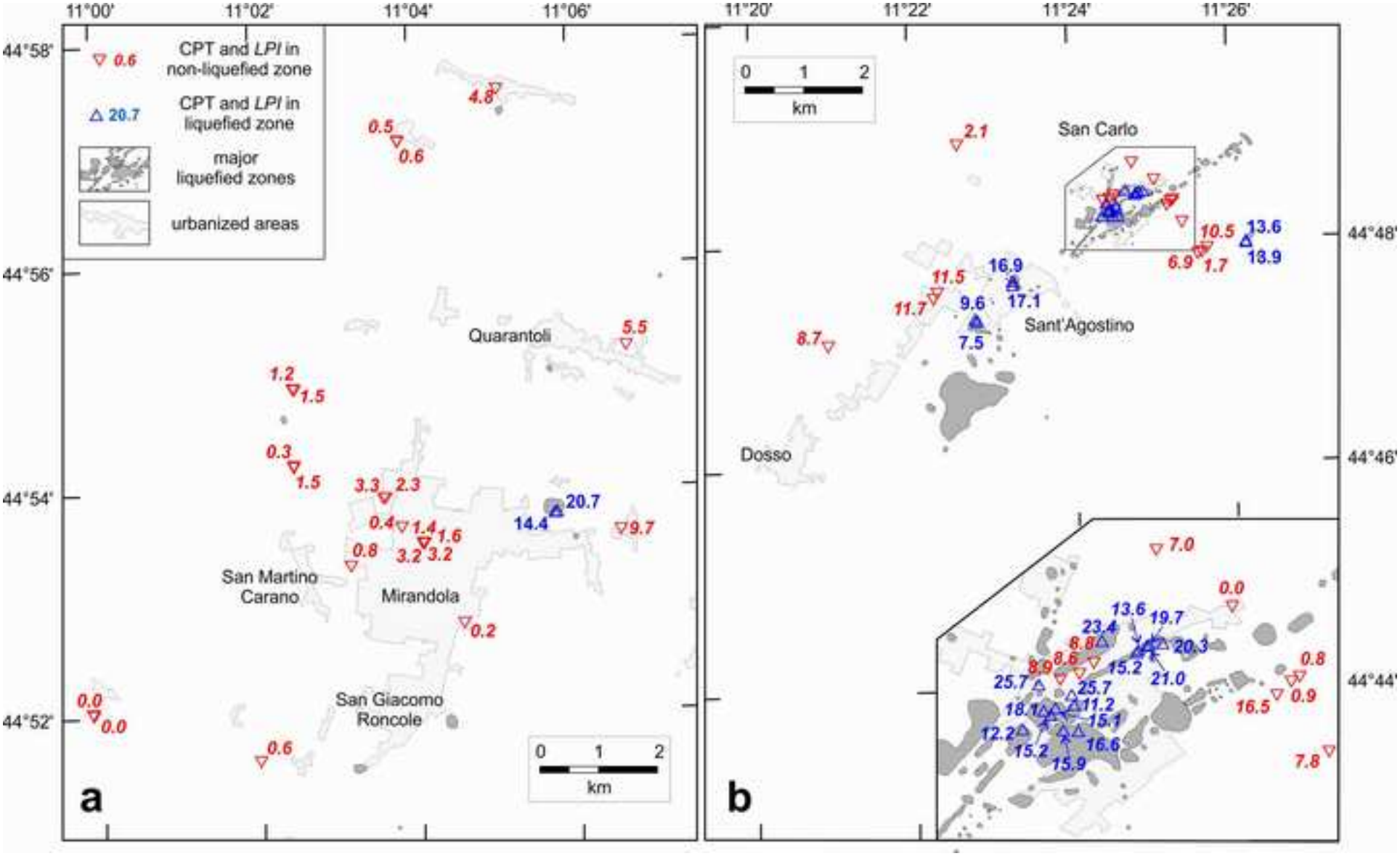

Figure

Click here to download high resolution image

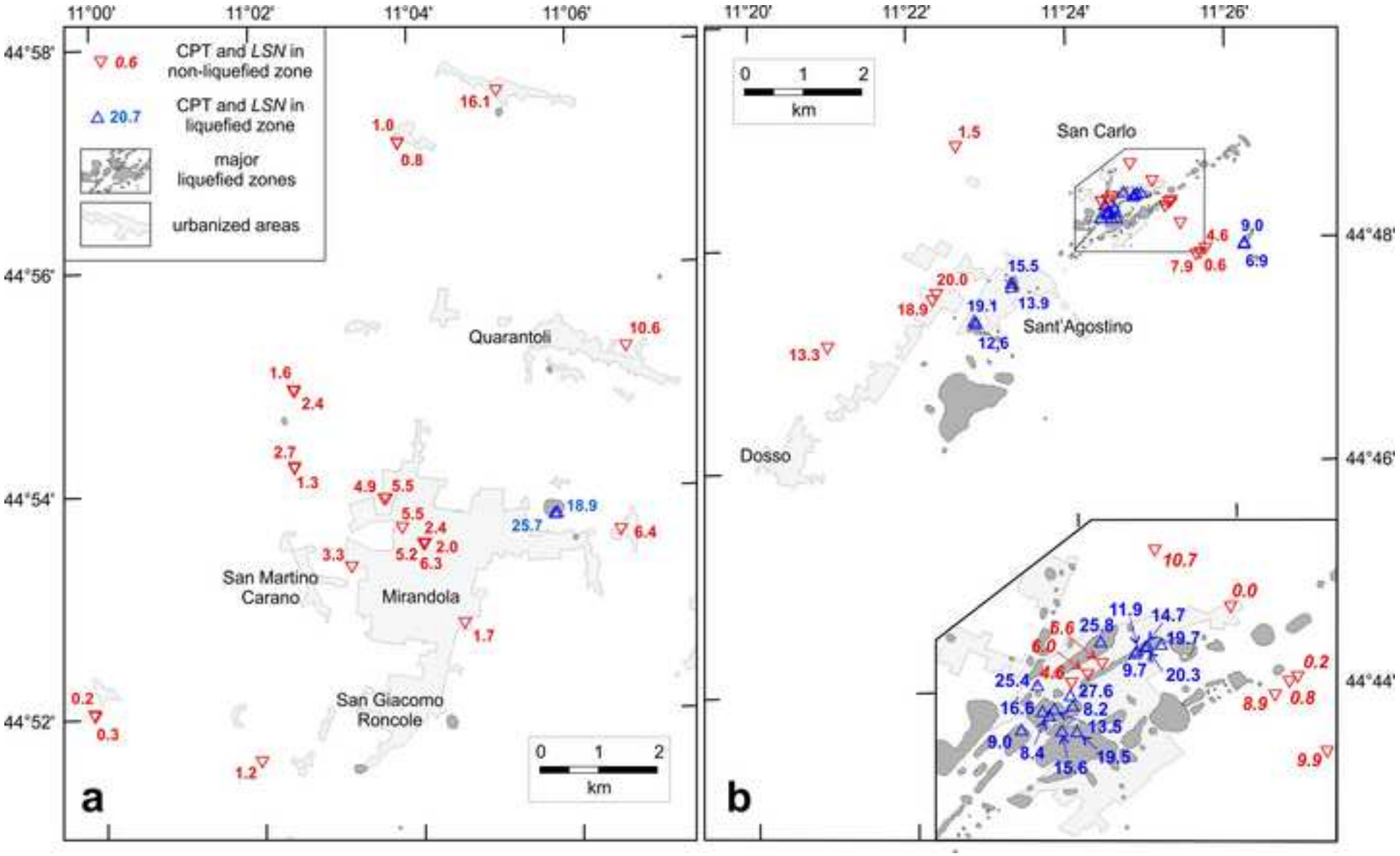

Figure

Click here to download high resolution image

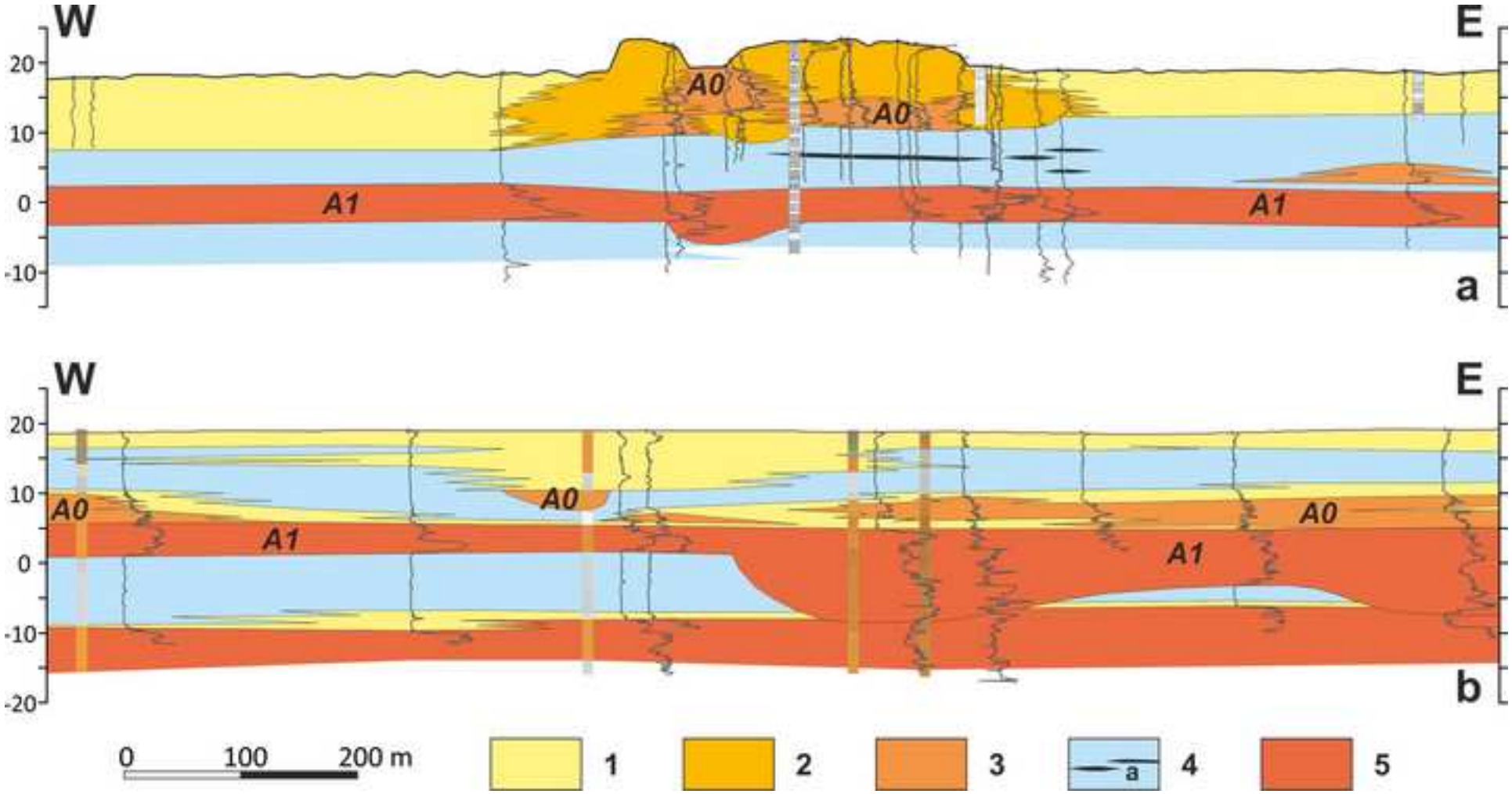

Figure

Click here to download high resolution image

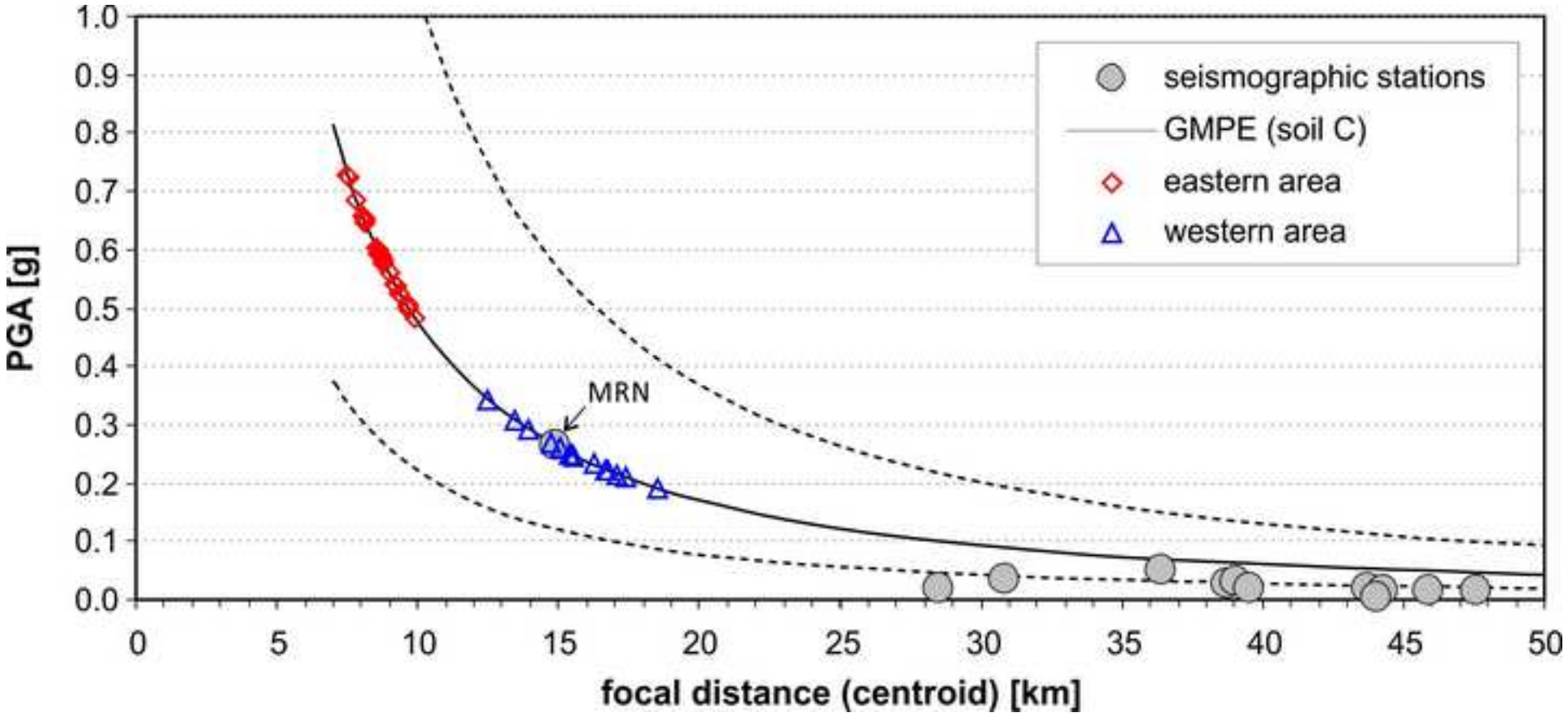

Figure

Click here to download high resolution image

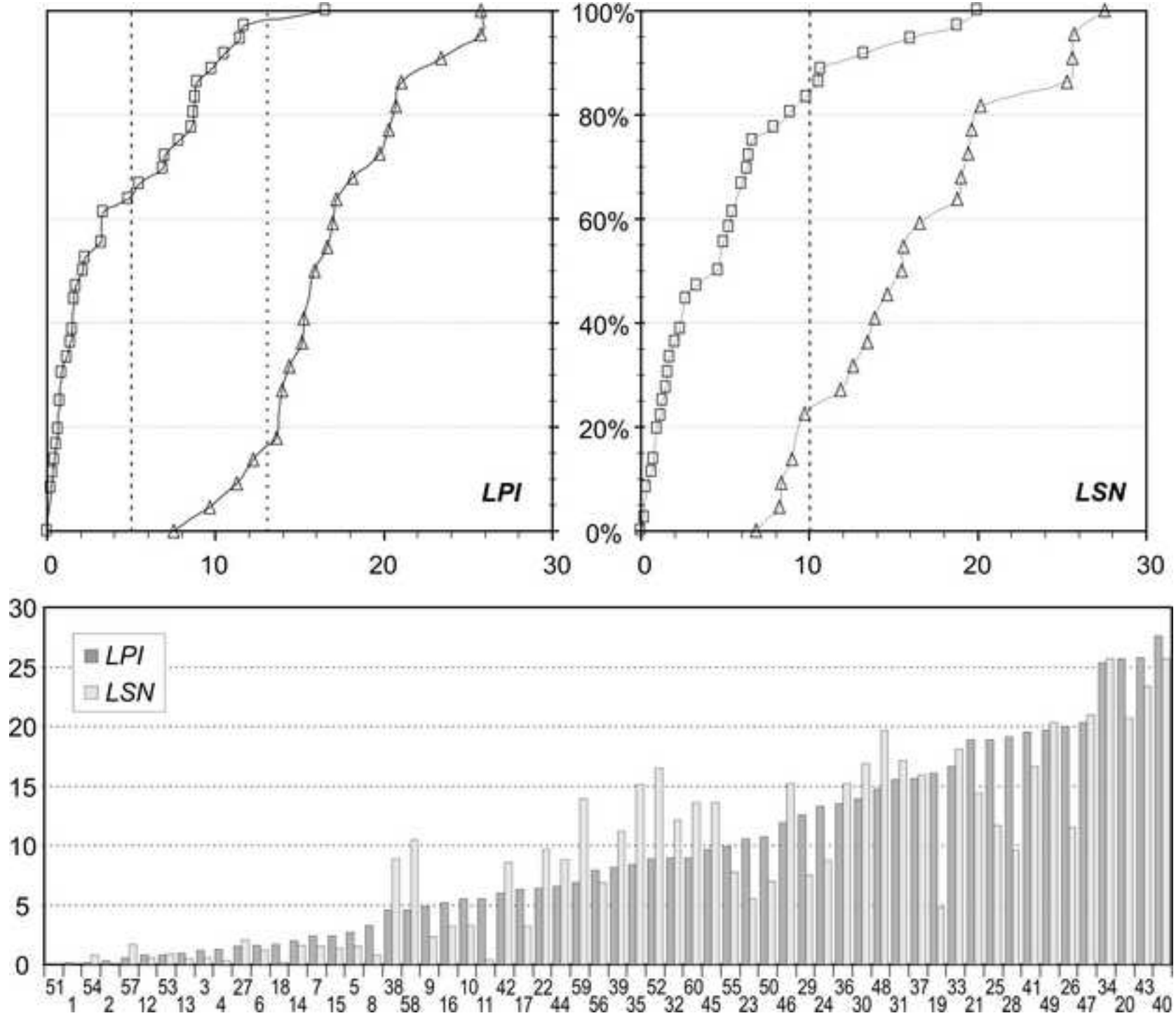

Figure captions

Figure 1: a) Tectonic sketch map of the buried Ferrara Arc and location of the May 2012 epicentral area. All marked faults are blind. The box indicates the enlarged map of Figure b. b) Epicentral area showing the liquefaction manifestations observed during post-event field surveys (Caputo and Papathanassiou, 2012; Papathanassiou *et al.*, 2012; Di Manna *et al.*, 2012; Emergeo WG, 2013). The stars indicate the instrumental epicentres of the May 20 (M_w = 6.1) and May 29 (M_w = 6.0) events (Pondrelli *et al.*, 2012; Massa *et al.*, 2013), the hexagons represent the corresponding macroseismic epicentres (Galli *et al.*, 2012), while the square is the surface projection of the slip plane centroid (Ganas *et al.*, 2012; Cesca *et al.*, 2013; Pezzo *et al.*, 2013). Continuous and dashed gray-scale contours represent the slip planes proposed by Ganas *et al.* (2012) and Pezzo *et al.* (2013), respectively. The triangle represents the Mirandola seismographic station (MRN) belonging to the national network, while the rhombs are the boreholes for the acquifers monitoring. The two black boxes indicate the investigated areas represented in Figures 8 and 9.

Figure 2: Examples of damages produced by the May 20, 2012 earthquake. a) broken pipelines; b) paved roads; c) buildings with cracking due to differential settlement; d) lateral spreading.

Figure 3: Examples of large-diameter water wells which locally enhanced the sand ejection during shaking and liquefaction of the sandy acquifer bodies.

Figure 4: Examples of ground loss due to liquefaction and consequent settlement of the builduings.

Figure 5: Examples of ground ruptures induced by lateral spreading phenomena occurring on top of an abandoned levee between San Carlo and Sant'Agostino. Fractures are several meters-long, arranged in complex overlapping and overstepping sets, characterized by horizontal opening up to 20 cm, sometimes by vertical displacements of 10-15 cm and locally by sand ejection.

Figure 6: Example of an incipient buckling process affecting the top layer(s) and due to differential horizontal movements triggered by lateral spreading phenomena.

Figure 7: Examples of bulging phenomena caused by the failed attempt of sand ejection due to the presence of a strong cap layer.

Figure 8: The *LPI* values calculated for the two investigated epicentral areas of Mirandola (a) and Sant'Agostino (b). See Figure 1b for locations.

Figure 9: The *LSN* values calculated for the two investigated epicentral areas of Mirandola (a) and Sant'Agostino (b). See Figure 1b for locations.

Figure 10: Representative sections across San Carlo (a) and Mirandola (b) areas based on penetrometric tests and cores. Note the strong lateral lithological variations occurring in the shallow subsoil and the different distribution of the sandy bodies in the subsoil of the two investigated areas. Legend: 1) silt and silt-clay (alluvial plain deposits from Apennines rivers); 2) silt-sand (proximal levee deposits); 3) main sandy bodies (channel deposits); 4) clay (marsh deposits) with peat lenses (a); 5) medium-corase sand (alluvial plain deposits of Po River). A0 and A1 indicate the semi-confined and the first confined acquifers, respectively (Rapti-Caputo and Martinelli, 2009; Molinari et al., 2007).

Figure 11: The PGA calculated as a function of the focal distance based on the GMPE proposed by Bindi *et al.* (2011; dashed curves are the $\pm\sigma$). Rhombs and triangles represent the test sites of the eastern and western epicentral areas, respectively. The circles indicate the PGA value measured during the May 20 mainshock at the several stations belonging to the Italian seismographic network (itaca.mi.ingv.it, last visited July 25, 2014). The record at the Mirandola station (MRN), which is the only one in the seismic near-field, is in perfect agreement with the predicted value.

Figure 12: Top: cumulative distribution of the *LPI* and *LSN* within the investigated areas. Squares and triangles correspond to penetration tests drilled in 'non-liquefied' and 'liquefied' zones, respectively, as observed in the field after the earthquake. The vertical dashed lines represent the different thresholds discussed in the text. Bottom: comparison between the *LPI* and *LSN* values calculated for the test sites. Numbers in abscissa correspond to Table 1 (first column)